American Institute of Aeronautics and Astronautics

AIAA-2003-5166

Progress in Development of Modeling Capabilities for a micro-Pulsed Plasma Thruster

Michael Keidar and Iain D. Boyd

University of Michigan

Erik L. Antonsen and Gregory G. Spanjers

Air Force Research Laboratory

39th AIAA/ASME/SAE/ASEE
Joint Propulsion Conference & Exhibit

20-23 July 2003
Huntsville, Alabama

AIAA-2003-5166

Progress in Development of Modeling Capabilities for a Micro-Pulsed Plasma Thruster

Michael Keidar and Iain D. Boyd

University of Michigan, Ann Arbor, MI 48109

Erik L. Antonsen*, and Gregory G. Spanjers**

Air Force Research Laboratory, Propulsion Directorate, Electric Propulsion Laboratory
Edwards AFB CA 93524

* University of Illinois U-C, Urbana, IL 61801
** Space Vehicles Directorate, Kirtland AFB, NM 87117-5776

Abstract

In this work we report on progress in the development of models for a Micro-Pulsed Plasma Thruster (μPPT) and its exhaust plume. As a working example we consider a μPPT developed at the Air Force Research Laboratory. This is a miniaturized design of the axisymmetric PPT with a thrust in the 10 μN range that utilizes Teflon™ as a propellant. The plasma plume is simulated using a hybrid fluid-PIC-DSMC approach. The plasma plume model is combined with Teflon ablation and plasma generation models that provide boundary conditions for the plume. This approach provides a consistent description of the plasma flow from the surface into the near plume. The magnetic field diffusion into the plume region is also considered and plasma acceleration by the electromagnetic mechanism is studied. Teflon ablation and plasma generation analyses show that the Teflon surface temperature and ablation rate are strongly non-uniform in the radial direction and have a maximum near the central electrode. As a result the propellant surface has the form of a cone with an apex at the central electrode. Analysis predictions for the ablation depth as well as the ablation profile shows close correspondence to experimentally observed dependencies. Long-term operation is associated with propellant and central electrode recession. To this end a model of the plasma flow inside of the anode tube is developed. Some preliminary results are reported. Electron and neutral densities predicted by the plume model are compared with near field plume measurements using a two-color interferometer and good agreement is obtained.

Introduction

Currently, pulsed plasma thrusters (PPT's) are considered as an attractive propulsion option for stationkeeping and drag makeup purposes for mass and power limited satellites[1]. In particular, the US Air Force has a growing interest in highly maneuverable microsatellites to perform various missions, such as space-based surveillance, on-orbit servicing, inspection, space control etc.[2] From a propulsion point of view, these missions require spacecraft propulsion systems that can deliver high thrust or high specific impulse. Recently, an electromagnetic PPT was successfully operated for pitch axis control on the EO-1 spacecraft.[3,4] A micro-PPT is another propulsion technology that has been designed at the Air Force Research Laboratory (AFRL) for delivery of very small impulse bit[2,5]. This is a simplified miniaturized version of a conventional PPT with a thrust in the 10 μN range designed to provide attitude control and stationkeeping for microsatellites. In this thruster, the discharge across the propellant surface ablates a portion of the propellant, ionizes it, and then accelerates it predominantly electromagnetically to generate the thrust. It is expected that the use of electromagnetic acceleration to create thrust will also lead to relatively high specific impulse.

Current development efforts on the micro-PPT concentrate on long-duration operation. It was found that the propellant and central electrode recede after several hours of operation. An important question is how micro-PPT operation changes over time because of this effect. Several parameters are very important such as ablation rate, thrust and plume properties. In parallel with an experimental study that is currently being conducting at AFRL, our aim is to model the micro-PPT operation under significant recession of the propellant and the central electrode.

In this paper we describe progress in modeling various aspects of the micro-PPT such as ablation, plasma generation and plasma flow in both flush and recessed modes. Model predictions are compared with recent measurements taken at AFRL.

Brief description of the AFRL Micro-PPT

Figure 1 shows a simplified schematic for a 2-electrode micro-PPT. A high voltage energy storage capacitor is connected directly to a coaxial propellant module. The propellant includes a central conductive rod that serves as the cathode in the discharge. The cathode is surrounded by an annulus of Teflon, which serves as the primary source of propellant. The Teflon propellant is then encased in a conductive tube, which serves as the anode. A DC–DC converter charges the capacitor to a high voltage. This voltage also appears at the electrodes and across the propellant face.

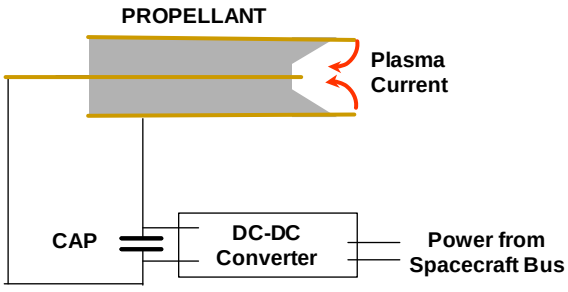

Figure 1. *Simple micro-PPT schematic*

Discharge of the capacitor can be initiated by an external ignitor plug, or in the self-triggering design the voltage on the electrodes can exceed the surface breakdown voltage of the propellant face. The surface discharge then ablates a small amount of the solid Teflon material, ionizes it, and accelerates it away from the thruster through primarily electromagnetic forces.

Flight versions of this thruster include a 3-electrode design, which uses an embedded, self-triggering tube to initiate a higher energy discharge in a larger electrode set. For the purpose of model validation, the experiments described here use only a two-electrode design with external ignitor.

Ablation and non-equilibrium ionization

In this section we focus on several aspects of plasma generation in the Micro-PPT. A schematic of the plasma-surface interactions near the propellant is shown in Fig. 2. It was shown recently that plasma conditions near the Knudsen layer edge strongly affect ablation. The effect consists in the flux of returned particles to the surface that is determined by the plasma density and temperature in the plasma bulk[6]. In principle, two limits are possible. When the plasma is very dense, the flux of returned particles is large. As a result, the velocity at the edge of the Knudsen layer is small. The opposite limit corresponds to the case when the plasma density is small. The plasma density and temperature depend on the flow conditions in the plasma bulk. One can expect that there is a smooth continuous transition between these two regimes.

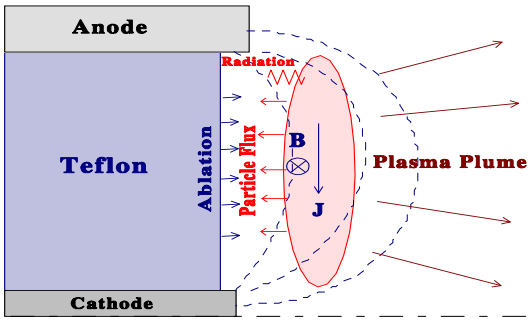

Figure 2: *Schematic of the plasma-surface interaction in a micro-Pulsed Plasma Thruster*

Let us briefly summarize the ablation model and peculiarities of the ablation in the presence of the magnetic field. Similarly to the previous works, we consider the multi-layer structure of the near surface region (see Fig. 3). There are two different characteristic layers between the surface and the plasma bulk: (1) a kinetic non-equilibrium layer adjacent to the surface with a thickness of a few mean free paths (the Knudsen layer), (2) a collision-dominated (hydrodynamic) layer.

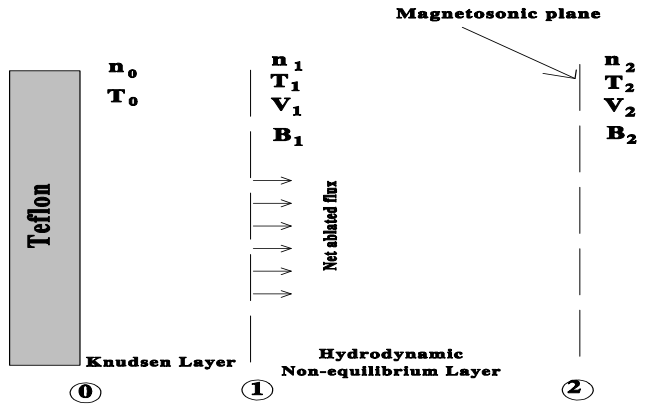

Figure 3: *Schematic of the near surface layers*

To simplify the present analysis, we assume that ionization equilibrium is reached near the edge of the second layer between boundaries 1 and 2. Therefore, the electron density at the boundary 2 will be calculated using Saha equilibrium. Solution of the hydrodynamic layer problem depends on the boundary conditions at the boundary 1, which is the Knudsen layer edge. To find the parameters at the edge of the Knudsen layer as a function of velocity at the Knudsen layer edge, V_1, we apply the mass, momentum and energy conservation equations in kinetic form. Corresponding relations between parameters at the edge of the Knudsen layer and those at the surface were presented elsewhere[7]. From the hydrodynamic equations one can readily obtain the velocity at the edge of the Knudsen layer:

$$V_1^2 = \frac{2kT_1}{m} \cdot \frac{\frac{n_1}{2} - \frac{T_2 n_2}{2T_1} + \frac{1}{4} \cdot \frac{\mu (jd)^2}{kT_1}}{\frac{3}{2} \cdot \frac{n_1^2}{n_2} - n_1} \quad \text{.....(1)}$$

where j is the current density and d is the thruster diameter; other parameters are defined in Fig. 3. The velocity V_1 as well as density n_1 determine the ablation rate: $\Gamma = m n_1 V_1$, where m is the heavy particle mass. The calculation of the velocity at the Knudsen layer edge is shown in Fig. 4 as a function of the discharge energy. The heavy particle density distribution in the acceleration region depends upon the specific geometry of the thruster and acceleration region. In order to study only general trends without details of the flow field in the acceleration region, we consider the total heavy particle density at the magnetosonic plane (boundary 2, Fig. 3) as a parameter.

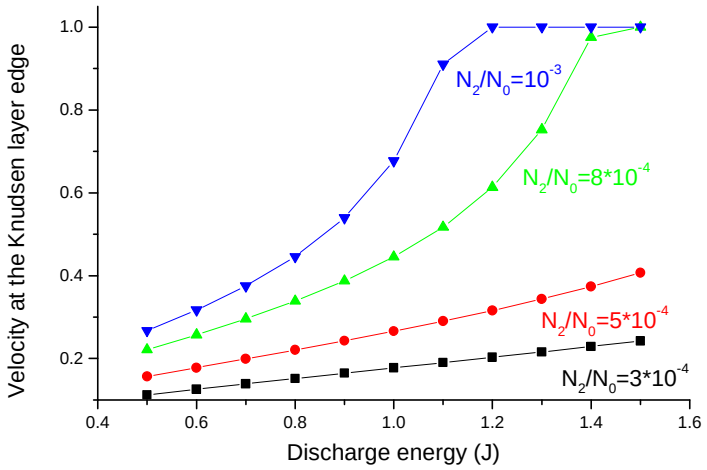

Figure 4: *Dependence of the velocity at the Knudsen layer edge on the discharge energy. The parameter is the ratio of the density at the magnetosonic plane to the equilibrium density*

One can see that the velocity V_1 increases with discharge energy and approaches its maximum value of the local sonic speed (as happens in the case of ablation into vacuum) for a certain energy. This happens

because stronger plasma acceleration leads to conditions close to the expansion into vacuum. It is expected that this effect should affect the ablation rate, since ablation rate is directly proportional to the velocity at the Knudsen layer edge. It will be shown later in the paper that this particular effect of strong velocity increase with current density may be responsible for a strong dependence of ablation rate on the discharge energy.

Let us now consider the plasma ionization. Previously it was found that accounting for non-equilibrium ionization helps to explain experimentally observed temporal behavior of the electron and neutral density in the near field plume.[8] The ionization layer can be physically determined as follows. At the beginning of the ionization layer the charged particle density is very small and therefore ionization becomes the primary process, since recombination has higher order dependence on the electron density. As the charged particle density grows, the recombination rate increases and near the edge of the layer the recombination rate becomes close to that of ionization thus establishing equilibrium. Therefore, in reality, the ionization layer edge is determined by recombination. A simplified way to attack the problem is to consider that in the steady or quasi-steady discharge, high plasma density and large electron temperature will lead to establishing a fully ionized plasma. Therefore the ionization layer is the region where transition to a fully ionized plasma occurs (see Fig. 5).

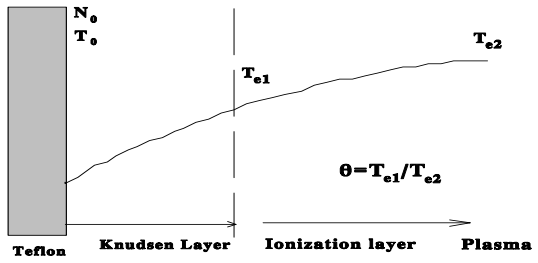

Figure 5*: Schematic of the near surface layers*

We start our consideration from the Knudsen layer edge. The reason for this is that at typical conditions, range the mean free path is much larger than the Debye length and therefore the sheath thickness is much smaller than the Knudsen layer length. It is assumed that electron impact ionization is the dominant process in the ionization layer, while recombination is unimportant. In this section we describe the asymptotic behavior of the solution of the ionization layer problem in the case of strong acceleration, i.e. strong effect of magnetic field in the ionization layer. This case corresponds to the micro-PPT conditions. We assume that the smooth sonic transition takes in the ionization layer. Using L'Hopital's rule one can find the velocity gradient near the sonic plane, which is finite under this condition. This procedure was used by a number of authors (see Refs. 9,10).

The solution that allows smooth transition has the following expression for maximal electron density (normalized by the total particle density) in the vicinity of the sonic point[8]:

$$n = 0.5(1 - \sqrt{1 - \frac{\alpha\beta}{\varepsilon^{0.5}}(1 - \frac{1}{\beta})}) \quad \text{..... (2)}$$

where n is the ratio of the electron density to the neutral density, $\alpha = C_{ia}/(r_a \alpha_i N_1)$; $\beta=(V_a/C_s)^2$; $\varepsilon=(T_i+T_e)/T_i$ and V_a is the Alfven speed:

$$V_a = \frac{B_1}{(\mu N_1 m)^{0.5}} \quad \text{..... (3)}$$

where C_{ia} is the heavy particle thermal velocity, B_1 is the magnetic field at the edge of the Knudsen layer. In order to calculate the ionization rate α_i for the C-F plasma, the electron impact ionization cross sections (available from a database[11]) are used. The Eq. 2 is an expression for the density behavior near the sonic plane in the case of regular sonic transition. According to the non-equilibrium model (Eq.2) the ionization degree is affected by an additional parameter, which is the ratio of the electron temperature at the beginning of ionization layer (in Eq. 2) to the electron temperature in the plasma bulk (see below).

The physical meaning of this parameter is that there is an electron temperature gradient from the plasma bulk to the propellant surface as shown in Fig. 5. Previously we used the ratio of the electron temperature at the beginning of the ionization layer to the bulk electron temperature θ as a parameter.[8] In this paper we will calculate the electron temperature distribution across the ionization region. The energy conservation equation in the ionization layer can be written

$$\frac{3}{2} n_e V \frac{dT_e}{dx} = \frac{j^2}{\sigma(T_e)} \qquad (4)$$

where V is the velocity, n_e is the electron density, j is the current density and σ is the plasma conductivity.

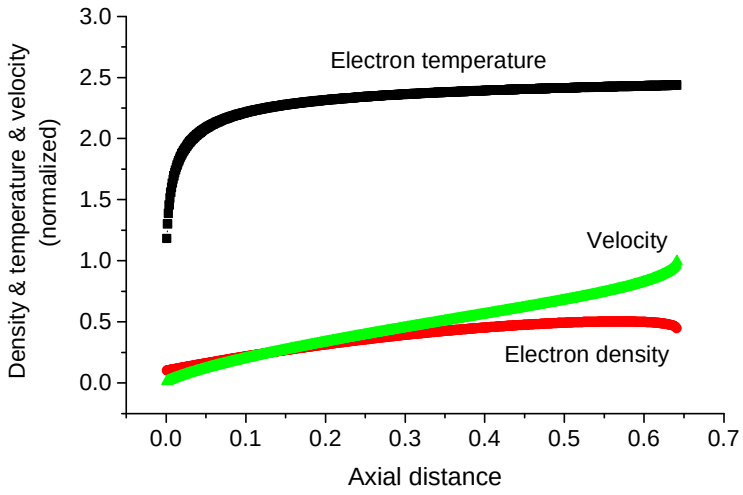

***Figure 6**: Typical parameter distribution along the ionization layer in the case of non-equilibrium ionization.*

An example of the parameter distribution across the ionization layer is shown in Fig. 6. One can see that generally the electron temperature increases by a factor of 2-2.5 from the beginning of the ionization layer towards the plasma bulk. In the present model of the non-equilibrium ionization, the electron temperature distribution across the ionization layer is taken into account.

Experimental data and comparison with model predictions

An experimental basis for comparison with the simulation results is provided using a two-color interferometer. Electron and neutral density measurements are taken for a 6.35 mm (1/4") diameter MicroPPT at AFRL. The interferometer uses 488 and 1152 nm wavelengths and a quadrature heterodyne technique described by Spanjers *et al.*[12] The two-color technique uses the difference in phase shifts from the two wavelengths to provide electron and neutral densities. This technique tends to ensure that both lasers are sampling the same portions of the plume.[13] Older data with less focusing is shown with typical uncertainty in Antonsen *et al*[14] along with a more thorough description of the two-color diagnostic. The data in Fig. 7 has a maximum uncertainty of $\pm 1.15 \times 10^{16}$ cm^{-3} for electron density and $\pm 1.76 \times 10^{16}$ cm^{-3} for neutral density at 2 μs into the discharge. For the data shown here, the beam center is located 3 mm from the fuel face on the thruster centerline with a beam diameter of 6 mm (thus measuring plasma density at the propellant face).

Figure 7 shows the experimental data co-plotted with model predictions. Plasma density peaks at about 2×10^{22} m^{-3} and decreases by several orders of magnitude towards the pulse end. The neutral density is significantly higher and peaks at about 14×10^{22} m^{-3}. The experimental data are taken at a discharge energy of 6.0 J from a 0.417 μF capacitor. A comparison of the simulation and experimental results can be seen in Fig. 7. One can see that the model satisfactorily predicts both the plasma and neutral density level and temporal behavior during the entire pulse.

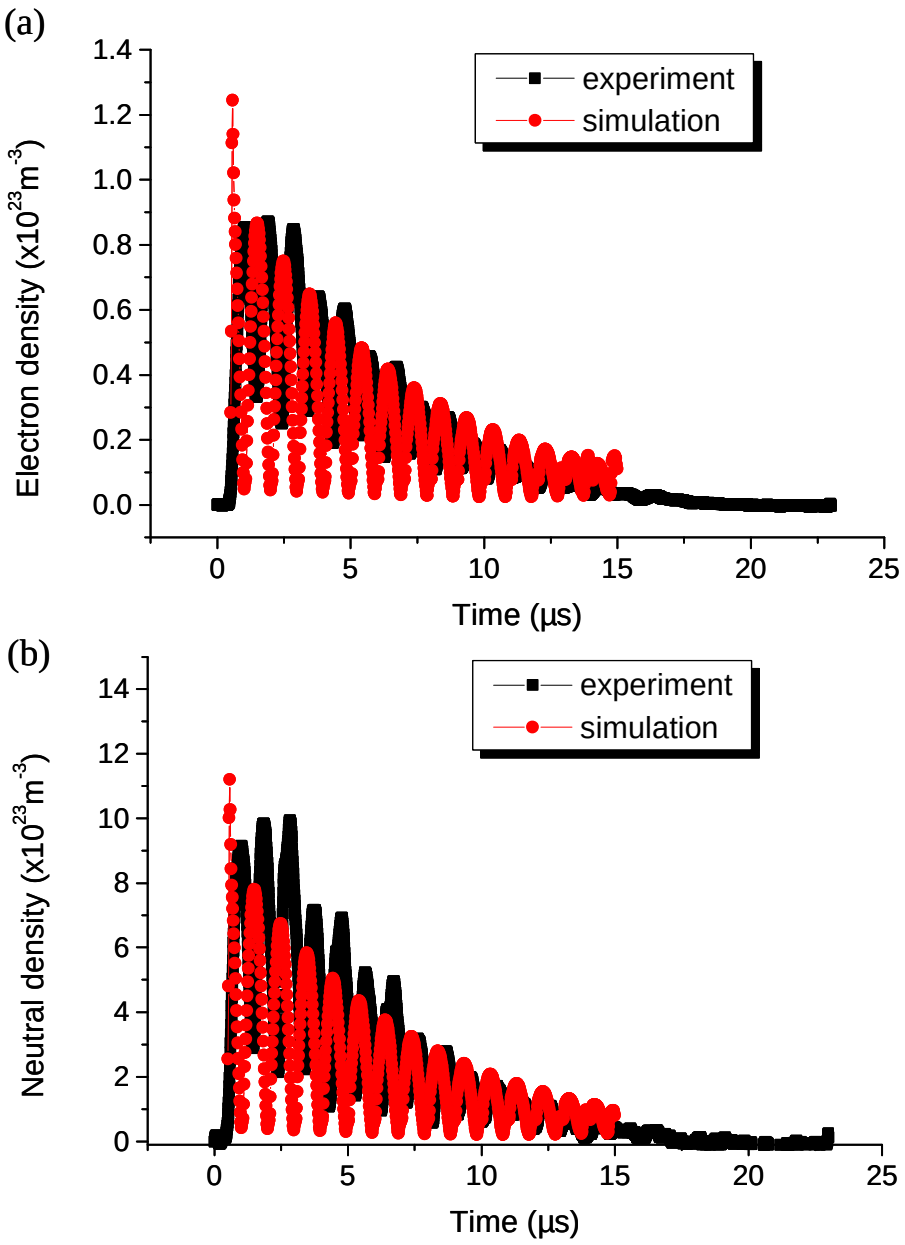

***Figure 7**: Electron (a) and neutral (b) density distribution. Comparison with experiment (in black).*

Propellant recession in micro-PPT. Magnetic field diffusion

In this section we describe the model of the plasma flow in the μPPT recessed mode. Let us start from the brief description of the particle model of the plasma flow in the PPT.

The plasma parameters at the thruster exit plane serve as boundary conditions for the plume model. The plume is modeled in the framework of a hybrid PIC-DSMC approach described elsewhere.[15] The general approach for the plume model is based on a hybrid fluid-particle approach that is described elsewhere.[16] In this particular model, the neutrals and ions are modeled as particles while electrons are treated as a fluid. Elastic (momentum transfer) and non-elastic (charge exchange) collisions are included in the model. The particle collisions are calculated using the direct simulation Monte Carlo (DSMC) method[17]. Momentum exchange cross sections use the model of Dalgarno *et al*.[18], while charge exchange processes use the cross sections proposed by Sakabe and Izawa[19]. Acceleration of the charged particles is computed using the particle-in-cell method (PIC).[20] A single grid employing non-uniform, rectangular cells is used for both the DSMC and PIC steps. Since the flow is assumed to be quasi-neutral, there is no requirement to resolve the Debye length. Hence, the cells are scaled by the local mean free path. A single time step given by the reciprocal of the maximum plasma frequency is used throughout. In order to calculate plasma expansion in the near plume region and plasma flow inside the tube (recessed mode) the magnetic field distribution must be calculated.

Previously our model was based on the assumption that electrons rapidly reach the equilibrium distribution and in the absence of the magnetic field can be described according to the Boltzmann relation[16]. While this was a satisfactory assumption in the case of an electrothermal thruster plume this is not suitable for the near field of an electromagnetic thruster. In the presence of a strong magnetic field,

the electron density distribution deviates from that according to Boltzmann[21]. In the case of a magnetic field the electron momentum equation reads (neglecting electron inertia):

$$0 = -eN_e(\boldsymbol{E}+\boldsymbol{V_e}\times\boldsymbol{B}) - \nabla P_e - N_e \nu_{ei} m_e(\boldsymbol{V}_e-\boldsymbol{V}_i) \quad \text{..... (5)}$$

We have assumed quasi-neutrality therefore $N_e = N_i = N$. Using the definition $\boldsymbol{j}=eN(\boldsymbol{V}_i-\boldsymbol{V}_e)$ the equation 5 is usually referred to as the generalized Ohm's law. The electric and magnetic field distributions in the plume can be calculated from the set of Maxwell's equations. We further assume that the magnetic field has only an azimuthal component and also neglect the displacement current. The combination of the Maxwell equations and electron momentum conservation gives the following equation for the magnetic field:

$$\partial\boldsymbol{B}/\partial t = 1/(\sigma\mu)\nabla^2\boldsymbol{B} - \nabla\times(\boldsymbol{j}\times\boldsymbol{B}/(eN)) + \nabla\times(\boldsymbol{V}\times\boldsymbol{B}), \quad \text{..... (6)}$$

where $\sigma=e^2N_e/(\nu_{ei}m_e)$ is the plasma conductivity which has only a weak dependence on the plasma density (in the Coulomb logarithm). Therefore it is assumed that plasma conductivity depends only on the electron temperature in the plasma plume. A similar approach was also recently employed in a plasma flow simulation of a PPT.[22] The electron temperature is calculated from the plasma layer fluid model.

It is assumed that the electrons are isothermal. Also, the Hall parameter is assumed to be small (this assumption will be verified below). It is assumed in Eq. 6 that the plasma conductivity is constant (mainly due to the fact that electron temperature is assumed to be constant in the near plume[7]) and that the density gradient does not affect the magnetic field diffusion. The last assumption comes from the fact that the

main density gradient is developed in the direction of magnetic field transport (as will be clear from the results below) and therefore does not affect magnetic field transport.[23]

A scaling analysis shows that the various terms on the right hand side of Eq. 6 generally may have importance in different regions of the plasma plume and therefore a general end-to-end plasma plume analysis requires keeping all terms in the equation. In the case of the near plume of the micro-PPT with a characteristic scale length L of about 1 mm, the magnetic Reynolds number $Re_m=\mu\sigma LV<<1$ (where V is the characteristic velocity ~10^4 m/s as shown below) and therefore the last term can be neglected. Taking this into account, Eq. 6 (in dimensionless form) can be written as:

$$Re_m \partial \mathbf{B}/\partial t = \nabla^2 \mathbf{B} - (\omega\tau)\{\nabla\times(\nabla\times\mathbf{B}\times\mathbf{B})\} \quad \text{..... (7)}$$

where $(\omega\tau)$ is the Hall parameter that measures the Hall effect. Therefore, depending on the plasma density, the Hall effect may be important for the magnetic field evolution. One of the first calculations of the plasma flow with Hall effect was performed by Brushlinski and Morozov (see Ref. 24 and references therein) who considered isothermal flow. The plasma density becomes high at the cathode and lower at the anode. The Hall effect has a particularly noticeable influence on the magnetic field distribution. The field near the anode increases and near the cathode decreases. As a result the current is deflected to the side and grazes the anode.

Our estimations show that the Hall parameter $\omega\tau<<1$ if the plasma density near the Teflon surface $N>10^{23}$ m^{-3}. This is usually the case in the micro-PPT (see the next section) so the Hall effect is expected to be small and will be not considered in this paper. Therefore the Eq. 7 is reduced to the simple magnetic transport equation. Having the magnetic field distribution one can calculate the current density distribution from Ampere's law:

$\mu \mathbf{j} = \nabla x \mathbf{B}$ ..... (8)

The magnetic field and current distributions calculated from this model are used in PIC to evaluate the ion dynamics. The ion velocity distribution depends upon the magnetic field distribution, and, the ion dynamics is calculated as follows:

$m d\mathbf{V}/dt = Z_i e(\mathbf{E} + \mathbf{V} \times \mathbf{B}) + \nu_{ei} m_e (\mathbf{V}_e - \mathbf{V}_i)$ ..... (9)

The electric field in this equation can be determined from the electron momentum equation (Eq. 5) and therefore the last equation reduces to the following simplified form:

$m dV/dt = \mathbf{j} \times \mathbf{B}/mN$..... (10)

A schematic of the recessed micro-PPT geometry and boundary conditions is shown in Fig. 8.

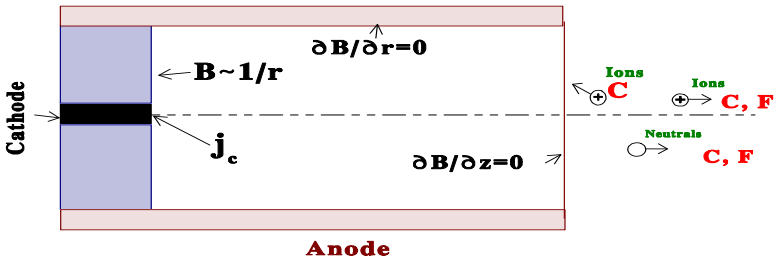

***Figure 8**: Schematic of the channel for a recessed micro-PPT*

Recession mode. Ablation rate

In the following, we show preliminary results for calculation of the magnetic field, current density and ablation rate during the discharge pulse. We consider a particular example of a micro-PPT with outer electrode (anode) diameter of 0.25 inch and operated at 6 J. The calculated magnetic field distribution is shown in Fig. 9. One can see that the magnetic field diffuses into a region of a few mm beyond the Teflon plane.

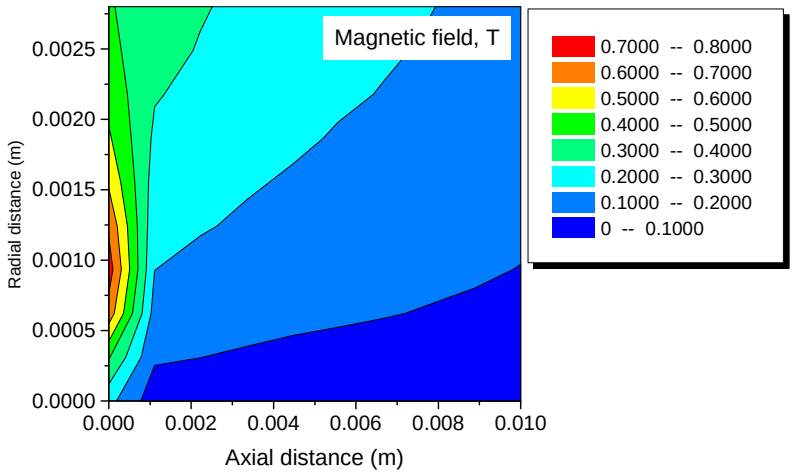

Figure 9*:Magnetic field distribution in micro-PPT acceleration channel (anode tube) near the current peak (t=2 μs)*

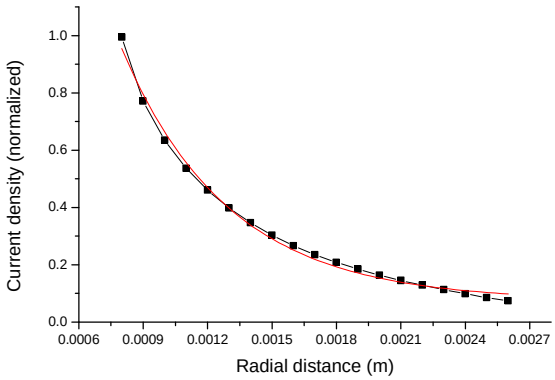

Figure 10*: Current density distribution (and fit) near the propellant face*

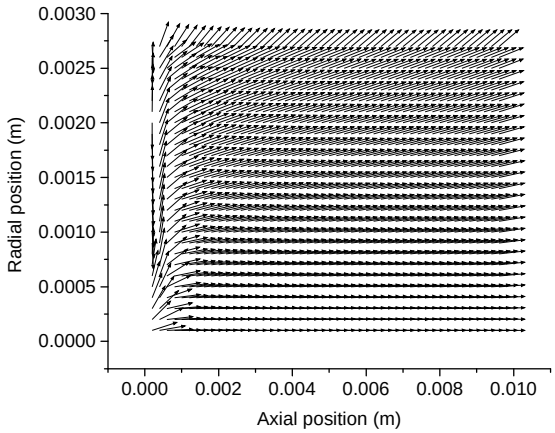

Figure 11*: Current density distribution (vector plot)*

The current density distribution near the Teflon surface corresponding to this magnetic field is shown in Fig. 10 and the vector plot is shown in Fig.11. Since Joule heating is the main source of heat flux transferred to the propellant one can expect that the Teflon ablation rate will depend on the radius. In fact the calculated ablation depth after a single pulse (Fig. 12) shows such a dependence. One can see that the expected recession depth is at a maximum near the central electrode. Similarly, a dependence of the recession depth on the radial position inside the tube is observed experimentally as shown in Fig. 13.

Experimental measurements of the recession cone are taken from a micro-PPT fired for 6 hours at 6 J and 1 Hz. The tube is soaked on one side in nitric acid, which eats away the copper leaving the Teflon intact. As half of the Teflon tube is exposed, the Teflon is shaved away exposing the conical recession pattern shown in Fig. 13. Reference lengths are measured from the copper tube lip back to the closest point of remaining Teflon and across the Teflon diameter. This yields the axes shown in Fig. 13. The DataThief program[25] is used to pick off the curve of the recession in a high-resolution picture.

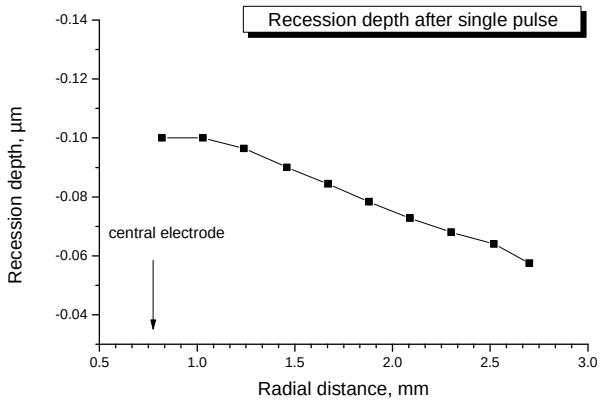

***Figure 12**: Model prediction of ablation depth after a single pulse*

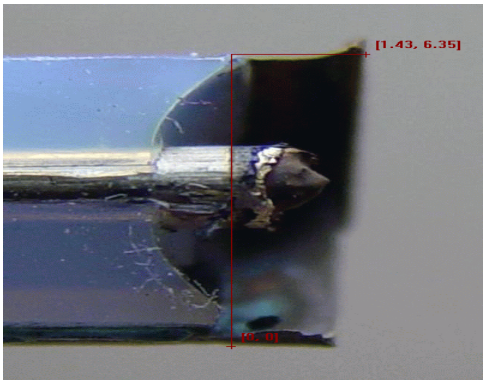

***Figure 13**: Typical ablation profile. 6 J*

Multiplying the computed ablation depth by the number of pulses one can calculate the total recession depth. These results are shown in Fig.14 where recession depth is plotted as a function of radial position within the tube. For comparison, the experimentally measured ablation profile obtained for the same conditions is also shown. It should be noted that the experimental ablation profile is not symmetrical as shown in Fig. 14 (two data sets). One can see that the calculated ablation depth as well as the ablation profile is close to that found experimentally.

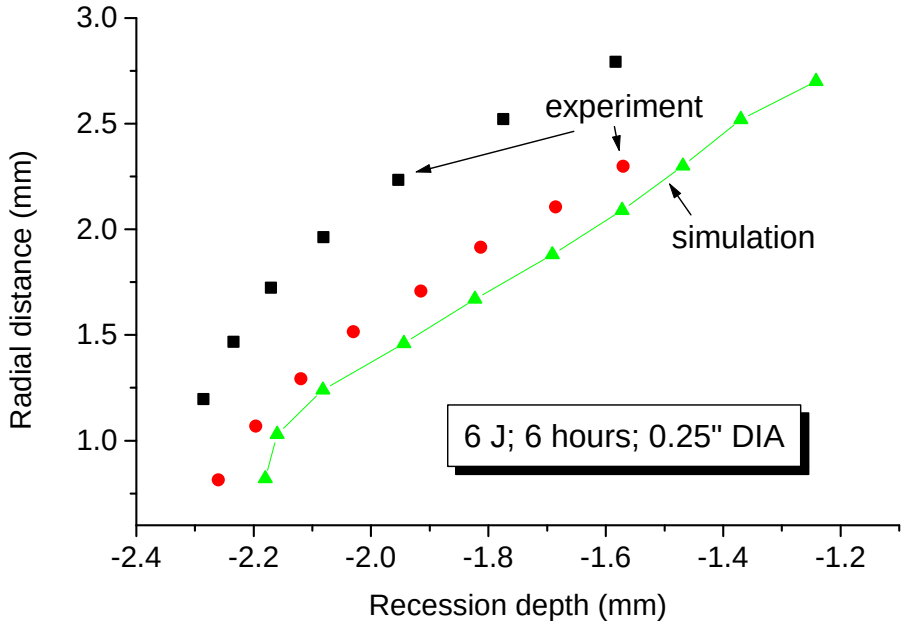

***Figure 14**: The dependence of the recession depth on the radial position within the tube after 6 h of firing and comparison with experimental profile. 6 J*

Recession mode. Plasma flow inside the tube.

The plasma generation and flow inside the anode tube during the recession mode are studied. The plasma parameters at the propellant face serve as boundary conditions for the plume model. The general approach for the plasma flow and the plume model is again based on a hybrid fluid-particle (PIC-DSMC) approach that was used previously for plasma plume expansion study.[15] In this model, the neutrals and ions are modeled as particles while electrons are treated as a fluid. In these calculations, we consider a particular example of a micro-PPT with outer electrode (anode) diameter of 0.25 inch and operated at 6 J. The plasma flow simulation is conducted for a total physical time of 15 μsec with output generated every 0.5

μsec. The maximum number of particles in these initial low-resolution simulations is 100,000 and the total computation time is about 9 hours.

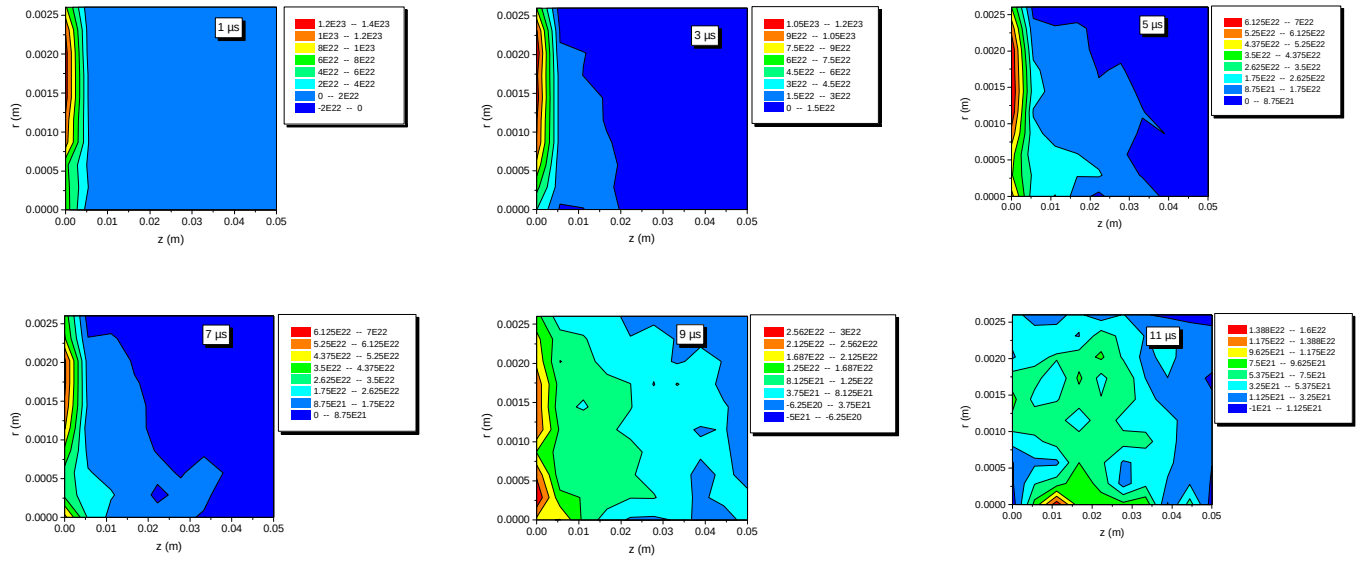

***Figure 15**: Plasma density distribution inside the tube*

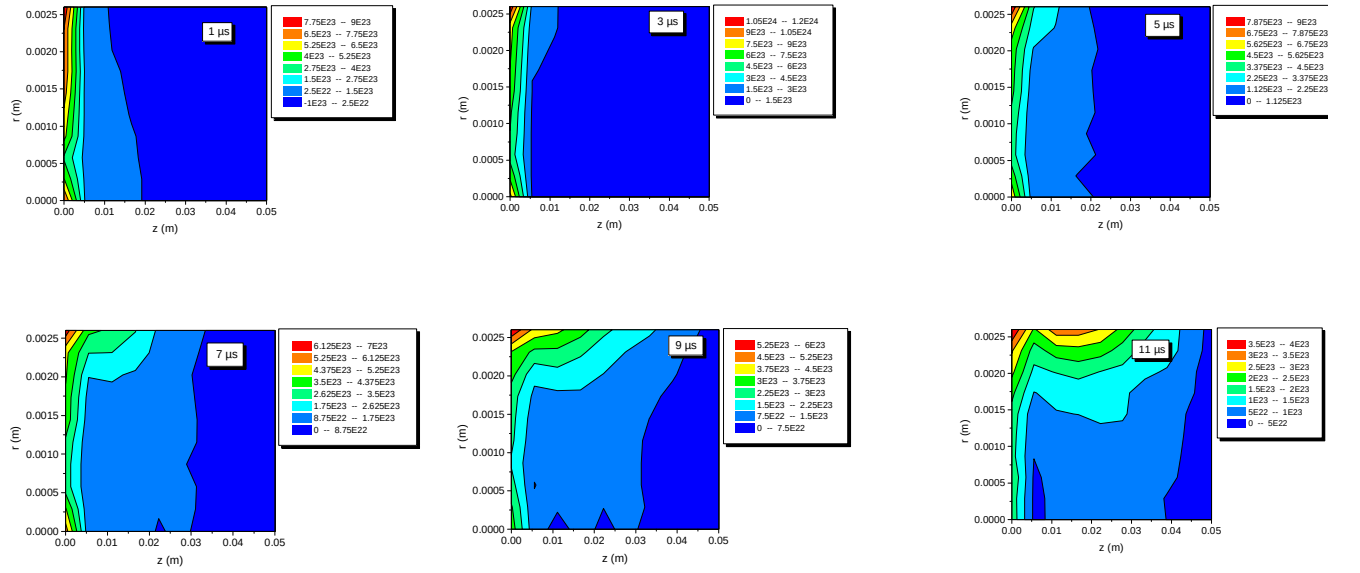

***Figure 16**: Neutral density distribution*

An example of plasma density evolution is shown in Figs. 15, 16 in the case of propellant recession of about 5 cm. It can be seen that plasma and neutral species have different behavior in the channel. One can see that the ionized species propagates from the propellant surface towards the thruster exit plane much faster than the neutral species. Plasma front propagates with average velocity of about 10 km/s. Plasma flux to the wall leads to ion neutralization at the wall. As a result, the neutral density increases near the outer wall.

Ablation rate dependence on the discharge energy

A common phenomenon in micro-PPT operation is arc-spoking. The plasma typically covers the entire central electrode, but attaches at specific points on the outer electrode resulting in an azimuthal non-uniformity of the discharge. Typically for past modeling efforts an azimuthally uniform current sheet has been assumed for simplicity in modeling, but experimental observations demonstrate that this is often not the case. Figure 17 shows pictures recorded by a high-speed camera showing the visible emission for a micro-PPT firing at several energies. The camera integrated the light signal through 20 μs which corresponds to the end of the current pulse for each firing.

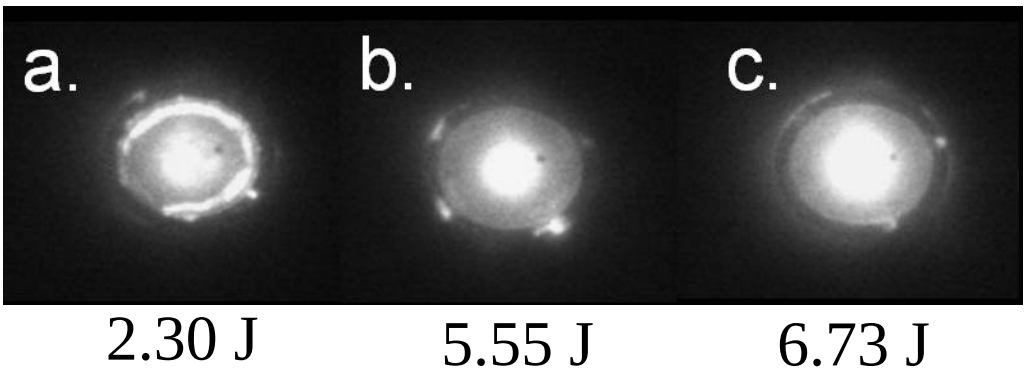

Figure 17*: Evidence of arc spoking in a 6.35 mm diameter micro-PPT*

At low energies the pictures indicate broad arc attachment around the outer electrode. As the discharge energy increases, specific locations are identified where the visible emission is localized. This is interpreted here as spoked arc attachment indicative of azimuthhal non-uniformity. Since the low energy regime results in char formation on the micro-PPT surface[26], typical thruster operation is in a regime where the arc is decidedly non-uniform. This non-uniformity is a possible source of non-monotonic behavior of the ablated mass with discharge energy. Let us try to evaluate possible effects related to non-uniformity as shown schematically in Fig. 18.

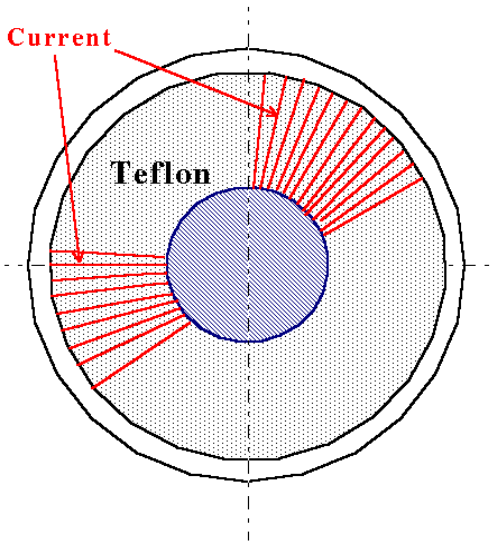

***Figure 18**: Propellant face showing current non-uniformity in the azimuthal direction*

If the discharge is non-uniform, the current density will increase locally. This in turn will lead to an increase of the heating of the plasma due to Ohmic heat (which is proportional to j^2). As a result, in the local areas of the discharge concentration, the heat fluxes to the propellant surface will increase that will in turn lead to locally high surface temperature and ablation rate. On the other hand, the ablated surface

area will be smaller and this may also affect the total ablation rate during the pulse. Let us now test this qualitative description using the previously described model. The simplest approach is to use a current density enhancement factor due to discharge non-uniformity as an input condition.

The calculated ablation rate in this case is shown in Fig. 19. As expected, the ablation rate increases with current density enhancement. However some saturation is predicted. This saturation is due to the fact that the propellant surface exposed to the ablation decreases accordingly and while the ablation rate in the area of the discharge concentration is higher, the total ablation rate tends to saturate.

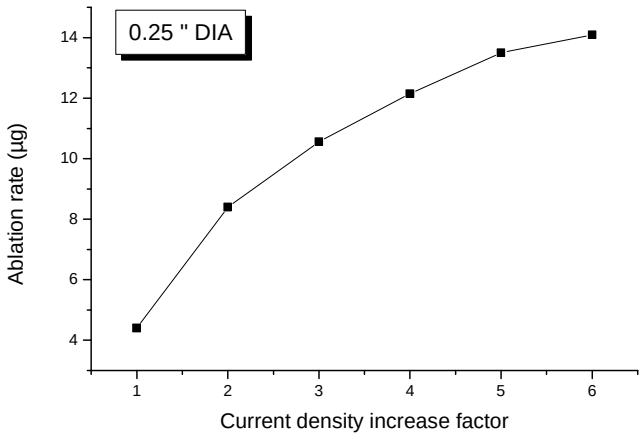

Figure 19*. Ablation rate dependence on current density increase due to discharge non-uniformity in the azimuthal direction.*

There are several physical reasons that may lead to discharge non-uniformity, such as current constriction, and cathode and anode spot appearance. The probability of all the mentioned effects increases as the discharge current increases. For instance it was shown[27] that a current increase in the several kA range leads to significant current constriction dependent on the plasma density distribution. The associated effects of the cathode and anode spot generation depend also on the current constriction. Therefore one

can expect that the discharge energy increase (and corresponding current increase) may lead to a high probability of current constriction that will generate azimuthal non-uniformity of the discharge.

One can conclude that discharge non-uniformity in the azimuthal direction may lead to significant changes of the thruster performance, such as ablation rate. The possibility of this effect increases with discharge energy. In order to study this effect a more general two-dimensional model of the propellant ablation and thermal conductivity of the propellant bulk must be developed. Conditions for the non-uniform discharge operation also need to be developed.

Concluding remarks

In this paper we reported on progress in the development of models for a Micro-Pulsed Plasma Thruster (μPPT). We considered end-to-end models that include plasma generation, flow and expansion in the near field. The magnetic field diffusion into the plume region was also considered and plasma acceleration by the electromagnetic mechanism was studied. Issues related to the long-term operation of the micro-PPT were studied, such as central electrode recession. Teflon ablation and plasma generation analyses showed that the Teflon surface temperature and ablation rate have a maximum near the central electrode. As a result the propellant surface has the form of a cone with an apex at the central electrode. Comparison of the model results for ablation depth as well as the ablation profile showed close correspondence to experimentally observed dependencies. In addition we presented an improved non-equilibrium ionization model that allows calculation of the plasma composition. Electron and neutral densities predicted by this model were compared with near field measurements using a two-color interferometer and good agreement was obtained. Finally discharge non-uniformity in azimuthal direction was studied both experimentally and theoretically. It was concluded that azimuthal non-uniformity (arc spoking) increases with discharge

energy and may lead to much stronger (non-linear) dependence of the ablation rate with discharge energy in a micro-PPT.

Acknowledgements

The authors gratefully acknowledge financial support by the Air Force Office of Scientific Research through grant F49620-02-1-0084 and by the Air Force Research Laboratory. We also acknowledge D. Bromaghim, V. Hruby, and L. Byrne for valuable discussions.

References

[1]R. A. Spores, R. B. Cohen and M. Birkan, "The USAF Electric propulsion program", *Proceeding of the 25th International Electric Propulsion Conference*, vol. 1, Worthington, OH, 1998, 1997, p.1.

[2] G. G. Spanjers, D. R. Bromaghim, Capt. J. Lake, M. Dulligan, D. White, J. H. Schilling, S.S. Bushman, E. L. Antonsen, R.L. Burton, M. Keidar and I. D. Boyd, "AFRL microPPT development for small spacecraft propulsion", *28th AIAA Joint Propulsion Conference*, Indianapolis, IN, USA, July 2002, Paper AIAA-2002-3974.

[3] J.W. Dunning, S. Benson and S. Oleson, "NASA's electric propulsion program", 27th Inter. Electric Prop. Conf., Pasadena, CA, IEPC-01-002, October 2001

[4] C. Zakrzwsky, S. Benson, P. Sanneman and A. Hoskins"On-orbit testing of the EO-1 Pulsed Plasma Thruster", 38th Joint Propulsion Conference, July 2002, Indianapolis IN, AIAA-2002-3973, July 2002.

[5] Spanjers, G.G., White, D., Schilling, J., Bushman, S., Lake, J., Dulligan, M., "AFRL MicroPPT Development for the TechSat21 Flight," 27th Intl Electric Propulsion Conference, IEPC paper 2001-166, Pasadena, CA 2001.

[6] M. Keidar, I.D. Boyd and I.I. Beilis, "*On the model of Teflon ablation in an ablation-controlled discharge*", J. Phys. D: Appl. Phys., 34, 2001, pp. 1675-1677.

[7] M. Keidar, J. Fan, I.D. Boyd and I.I. Beilis, "Vaporization of heated materials into discharge plasmas", *J. Appl. Phys*., 89, 2001, pp. 3095-3098.

[8] M. Keidar and I.D. Boyd, Ionization non-equilibrium and ablation phenomena in a micro-pulsed plasma thruster, *28th AIAA Joint Propulsion Conference*, Indianapolis, IN, USA, July 2002, Paper AIAA-02-4275.

[9] A. Fruchtman, N. J. Fisch, and Y. Raitses, Control of the electric field profile in the Hall thruster, Phys. Plasmas, 8 No. 3, pp. 1048-1056 (2001)

[10] E. Ahedo, P. Martinez-Cerezo, and M. Martinez-Sanchez, One –dimensional model of the plasma flow in a Hall thruster, Phys. Plasmas, **8** No. 6, pp. 3058-3067 (2001)

[11] IAEA Aladin database (http://www-amdis.iaea.org/aladdin.html)

[12] G.G. Spanjers, K.A. McFall, F. Gulczinski III, R.A. Spores, "Investigation of Propellant Inefficiencies in a Pulsed Plasma Thruster, AIAA Paper 96-2723, July 1996

[13] E.L. Antonsen, Herriott Cell Interferometry for Pulsed Plasma Density Measurements, MS Thesis, University of Illinois at Urbana-Champaign, 2001

[14] Antonsen, E., Burton, R., Spanjers, G.G., "*High Resolution Laser Diagnostics in Millimeter-Scale Micro Pulsed Plasma Thrusters*", 27th Intl Electric Propulsion Conference, IEPC paper 2001-157, Pasadena, CA October 2001.

[15] M. Keidar and I.D. Boyd, Electromagnetic effects in the near field plume exhaust from a pulsed plasma thruster", *27th AIAA Joint Propulsion Conference*, Salt Lake City, UT, USA, July 2001, Paper AIAA-01-3638.

[16] I. D. Boyd, M. Keidar, and W. McKeon, Modeling of a pulsed plasma thruster from plasma generation to plume far field, *Journal of Spacecraft and Rockets, Vol. 37, No. 3, 2000.*

[17] G.A. Bird, "*Molecular gas dynamics and the direct simulation of gas flows"* (Clarendon Press, Oxford, 1994).

[18] A. Dalgarno, M.R.C. McDowell and A. Williams, The modilities of ions in unlike gases, Proc. Of Royal Soc. Of London, Vol. 250, April 1958, pp. 411-425.

[19] S. Sakabe and Y. Izawa, Simple formula for the cross sections of resonant charge transfer between atoms and their ions at low impact velocity, Physical Rev. A: General Physics, v. 45, No. 3, 1992, pp. 2086-2089.

[20] C.K. Birdsall and A.B. Langdon, Plasma Physics via Computer Simulation, Adam Hilger Press, 1991.

[21] I.I. Beilis, M. Keidar and S. Goldsmith, "Plasma-wall transition: The influence of the electron to ion current ratio on the magnetic presheath structure", Physics of Plasmas, 4, 1997, pp. 3461-3468.

[22] G.A. Popov, M.N. Kazeev, V.F. Kozlov, "Two dimensional numerical simulation of coaxial APPT", 27th Intl Electric Propulsion Conference, IEPC paper 2001-159, Pasadena, CA October 2001.

[23] A.S. Kingsep, Yu.V. Mokhov and K.V. Chukbar, "Nonlinear skin effect in plasmas", Sov. J. Plasma Phys., 10(4) 1984 pp. 495-498.

[24] K.V. Brushlinskii ans A.I. Morozov, "Calculation of two-dimensional plasma flows in channels", in Rev. Plasma Physics, Ed. M.A. Leontovich, Volume 8, 1980, Consultants Bureau, New York.

[25] http://ioc.unesco.org/oceanteacher/resourcekit/M3/Toolbox/datathief.htm

[26] M. Keidar, I. D. Boyd, F. S. Gulczinski, E. L. Antonsen, and G. G. Spanjers, "Analyses of Teflon Surface Charring and Near Field Plume of a Micro-Pulsed Plasma Thruster," IEPC Paper 01-155, October 2001.

[27] I. Beilis, M. Keidar, R. L. Boxman, and S. Goldsmith. Theoretical study of plasma jet expansion in a magnetic field in a disc anode vacuum arc. *J. Appl. Phys.*, 83 (2), 1997, pp. 709-717.